Consistent optical imaging and color measurement of the skin

Yves Vander Haeghen[ab], J.M. Naeyeart[a], I. Lemahieu[b]

[a]Dept. Engineering, ELIS-MEDISIP, Univ. Gent, St.-Pietersnieuwstr. 41, 9000 Gent, Belgium

[a]Dept. Dermatology, Univ. Hospital, De Pintelaan 185, 9000 Gent, Belgium

ABSTRACT

We propose a small field-of-view color image acquisition system for the imaging and measurement of skin lesion and its properties in dermatology. The system consists of a 3 chip CCD camera, a frame grabber, a high-quality halogen annular light source and a pentium PC. The output images are in a standard device-dependent color space called *sRGB* or ITU-R BT.709 which has a known relation to the device-independent CIE XYZ color space and provides a fairly realistic view on a modern CRT-based monitor. In order to transform the images from the unknown and variable input RGB color space of the acquisition system to the sRGB space a profile of the acquisition system is determined based on 24 color targets with known properties. Determination of this profile is simple and quick, and it remains valid for many hours of operation (weeks or even months of normal use). Precision or reproducibility of the system is very good, both short-term (consecutive measurements) $\langle \Delta E^*_{ab} \rangle = 0.04$ with $\Delta E^*_{ab} < 0.1$, medium-term (measurements under one profile but on different warm-up cycles) $\langle \Delta E^*_{ab} \rangle = 0.34$ with $\Delta E^*_{ab} < 1.2$. Long-term precision (measurements under different profiles) is of the same order. Accuracy was evaluated for profiles based on different RGB to $sRGB$ polynomial transforms computed both by linear least-squares in the $sRGB$ space and by non-linear optimization in CIE $L^*a^*b^*$ color space. Results show that, using a set of test targets consisting of 15 paper color targets and 12 real measurements of human skin, the simple linear transform outperforms higher order polynomials and has $\langle \Delta E^*_{ab} \rangle = 6.53$, with $\Delta E^*_{ab} < 11.21$. A small study of the pigmentation of the human skin after UV-radiation shows that when measuring areas of at least a few hundred pixels differences of more than 2-3 dE units are statistically significant.

Keywords: Color calibration, Dermatology, Color image acquisition, camera calibration, Colorimetry, CIE $L^*a^*b^*$

1. INTRODUCTION

In dermatology color and color difference often convey important diagnostic information, especially when investigating pigmented lesions and more particularly skin cancer. In order to make quantitative color measurements on irregular and variable sized skin lesions, standard chromameters or spectrophotometers are generally useless because of their fixed aperture. Traditional photography has the benefit of providing a visual record of the lesion, but doesn't have very consistent color reproduction due to differences in film, illumination and development. Although in digital photography no film is involved, it is not straightforward to obtain a constant response from a digital image acquisition system.[1,2] Moreover, most digital cameras are not colorimetric, i.e. their color sensors don't have spectral response functions that are proportional to the CIE $\bar{x}\,\bar{y}\,\bar{z}$ color matching functions (CIE stands for 'Commission Internationale de l'Eclairage', a standardizing body in the field of color science). This means it is not easy to compute perceptual color differences because the relation between the device-dependent input RGB space and the device-independent CIE XYZ space or a related color space e.g. $sRGB$ is unknown and has to be determined. This subject was already extensively covered in the literature,[3,4,2,5–9] but here the emphasis is clearly on a simple and practical scheme, making no pretense at being a color appearance model or at color constancy. The use of digital photography in dermatology has already been investigated several times, mostly using device-dependent color spaces, e.g. RGB and HSV.[10–13] Sometimes device-independent color spaces were used,[14,15] although it is unclear just how the necessary transform was obtained. At present no system for use in dermatology has been proposed that uses a standard color space with known primaries and white point. Such a color space has the additional benefit of allowing the interchange of images for more than just viewing purposes, and opens perspectives in the area of tele-medicine.

E-mail: Yves.VanderHaeghen@rug.ac.be

2. THE ACQUISITION SYSTEM

The acquisition system consists of a JVC KY-55B 3-chip CCD camera with a Pentax manual zoom lens, a Schott* KL1500 150 Watt halogen light source and an Integral Technologies†, FlashPoint 128 frame grabber. The field of view of the CCD camera is 2.0 cm by 1.5 cm. With an image containing 760 by 570 pixels the resolution is 38 pixels/mm. The light source is linked by a 2 m long optical fiber to a continuous ring-light that fits around the zoom lens. A blue filter changes the color temperature of the light source from 2800 K to around 6500K, making it a rough approximation of the CIE D65 white-point of the sRGB color space. This avoids metamerism problems related to the difference between the light source and the white point of the output color space. The frame grabber is fitted in a standard 150 MHz Pentium PC running Windows 95, and acquisition is done using the PAL analog RGB format which is digitized with 8-bit precision per color channel. The settings of the CCD camera can be adjusted through the serial port of the PC. The settings of the frame grabber are controlled using the FlashPoint Software Developer's Toolkit 3.0 from Integral Technologies. The color targets are taken from the MacBeth Color Checker Chart‡ (MBCCC).

3. DETERMINING THE ACQUISITION SYSTEM PROFILE

The calibration of the whole acquisition system consists of several consecutive steps: determination of the camera offset, the frame grabber offset, the frame grabber gain, the camera aperture, the color gains of the camera, the linearizing look-up table, and finally the transform from the unknown device-dependent acquisition system RGB space to standard device-dependent sRGB space. The aim of all but the last two steps is to maximize the dynamic range and resolution of the acquisition system. All these settings are stored in a so-called profile of the acquisition system. Before discussing each of these steps the simple camera and frame grabber models upon which they are based are reviewed.

3.1. The camera and frame grabber model

The output voltage V_c^{cam} of the camera for a certain color channel $c = R, G, B$ and for a certain pixel i can be written as:

$$V_{c,i}^{cam} = \Psi_0^{V_{max}^{cam}} \left([V_{offset}^{cam} + g_c^{cam} (V_{c,i}^{CCD} + V_{dark}^{CCD})]^{0.45} \right), \tag{1}$$

with V_{offset}^{cam} a variable offset voltage, $V_{c,i}^{CCD}$ a voltage proportional to the light incident on the element corresponding with the same pixel in the CCD array of color channel c, and V_{dark}^{CCD} the voltage resulting from the very temperature sensitive CCD dark current; g_c^{cam} is a variable color channel dependent gain, which is always 1 for the green channel. This is the reason the green channel will always be used in determining color channel independent parameters. The function $\Psi_0^{V_{max}^{cam}}$ represents the clipping that occurs when an output voltage is out of range:

$$\Psi_0^{V_{max}}(V) = \begin{cases} 0 & \text{if } V < 0 \\ V & \text{if } 0 \leq V \leq V_{max} \\ V_{max} & \text{if } V > V_{max} \end{cases}. \tag{2}$$

The 0.45 power dependence is called the gamma correction, and is a compensation for the 2.2 power law in the transfer function of a CRT relating electron gun input voltage and light intensity. It allows the camera to drive a CRT directly and can generally be turned on or off. Similarly, the human visual system (HVS) is also highly non-linear when relating visual impressions with the physical properties of light, and is governed by a 1/3 power-law. Basically, the HVS is much more sensitive at low than at high light intensities. This causes problems when trying to digitize linear-light RGB signals and in order to avoid visible quantization errors for dark colors at least 12 bits are needed. Because by coincidence the HVS and CRT transfer functions are almost each others inverse, visual resolution is much more constant at all intensity levels for gamma-corrected RGB ($R^*G^*B^*$) signals and it is possible to digitize them at 8 bits without too much errors[16] (to be precise we should use luminance instead of intensity). Digitized $R^*G^*B^*$ values can be converted numerically to single-precision linear RGB values using a 2.2 power-law (inverse

*Shott Glaswerke, Hagenauer strasze 38, D-65203 Wiesbaden
†Integral Technologies, Inc, 9855 Crosspoint blvd, Suite 126, Indianapolis, Indiana, 46256 USA
‡Macbeth, 405 Little Britain rd, New Windsor, NY 12553-6148, USA

gamma-correction) when needed. The 8-bit digitized R*G*B* pixel value P_c^* of the frame grabber and the linear RGB pixel value P_c may thus be written as:

$$\begin{aligned} P_c^* &= \Re\left(255\frac{\Psi_0^{V_{max}^{fg}(V_{offset}^{fg}+g^{fg}V_c^{cam})}}{V_{max}^{fg}}\right) \\ P_c &= \left(\frac{P_c^*}{255}\right)^{2.2}, P_c \in [0\ 1.0]. \end{aligned} \tag{3}$$

with V_{offset}^{fg} again a variable offset voltage, g^{fg} the variable frame grabber gain and $\Re$ the integer rounding operator. In reality (1) and (3) depend on more variable parameters, but these are not relevant to the proposed scheme. The camera parameters V_{offset}^{cam} and g_c^{cam} can be set using values in the range [0, 255], while the frame grabber values for V_{offset}^{fg} and g^{fg} have to be in the range [0, 63]. The relationship between these values and the variable parameters is linear.

3.2. The camera offset voltage

The aim is to make sure that a totally non-reflecting target, i.e. a target with reflective luminance $Y = 0$, results in $V_G^{cam} = 0$. Turning the light source off, closing the lens diaphragm and putting the lens cap on provides us with such a target. As no other parameters of the acquisition system have been properly set so far we cannot determine an aim pixel value P_G^* or P_G for the target. We therefore adopt the following scheme:

1. Make sure the target produces a non-zero image averaged green pixel value $\langle P_G \rangle$ by setting a high frame grabber gain and offset.
2. Measure $\langle P_G \rangle$ in function of the camera offset voltage parameter.

It can be seen using (1) and (3) that this will result in a curve consisting of two straight lines: one horizontal line as long as $V_{offset}^{cam} \leq -g_c^{cam} V_{dark}^{CCD}$, and one sloping line once clipping no longer occurs and $V_{offset}^{cam} \geq -V_{dark}^{CCD}$ (see fig. 1). At the setting at which the two lines intersect the offset voltage exactly compensates for the voltage resulting from the dark current, and $V_G^{cam} = 0$. To determine this point reliably and independently of the frame grabber settings we fit a horizontal and a sloping straight intersecting at each of the offset voltage settings through the data, and compute the fitting errors. The desired setting is the one with the lowest error (see fig. 1). We will refer to this operation as the two-line intersection method.

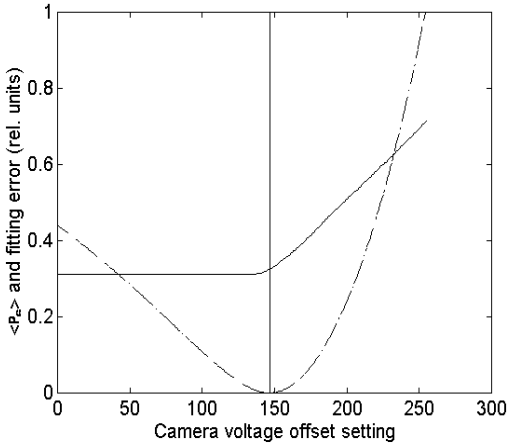

Figure 1. The image averaged linear pixel value for the green channel in function of the camera voltage offset setting (solid line) and the corresponding fitting errors (dashed line). The setting with the smallest fitting error is indicated by the vertical solid line.

3.3. The frame grabber offset voltage

Next we determine the setting of the frame grabber offset voltage so that $\langle P_G^* \rangle = \langle P_G \rangle = 0$. Because $V_G^{cam} = 0$ for the $Y = 0$ target, $\langle P_G^* \rangle$ is independent of the frame grabber gain g^{fg}. This means theoretically we only have to find the highest offset voltage setting at which $\langle P_G^* \rangle$ is zero. However, we still favor the two-line intersection method as being more robust and general. It is important to note that because the camera signal V_G^{cam} doesn't change but is digitized with another offset voltage only P_G^* has a piecewise linear relationship with the offset voltage, and not P_G!

3.4. The frame grabber gain and camera lens aperture

In order to maximize the dynamic range of the camera we wish that $\langle P_G^* \rangle = 255$ for a perfectly reflecting target ($Y = 100$), given the light source. This can be achieved in two steps. First g^{fg} is set so that the maximal camera signal V_{max}^{cam} is digitized as 255. For this the camera CCD's are saturated by fully opening the lens aperture, and measuring the highly reflecting MBCCC 'white' target. Then $\langle P_G \rangle$ is measured in function of g^{fg} and the two-line intersection method is again used to determine the optimal gain setting. Secondly, the continuous aperture of the lens is adjusted manually until $< P_G^* >= 255 \frac{Y_{white}}{100}^{0.45}$ for the same 'white' target.

3.5. The camera color balance and linearizing look-up table

The aim of these two operations is to obtain a linear response from the acquisition system for series of color targets with the same chromaticity coordinates $\frac{X}{X+Y+Z}$ and $\frac{Y}{X+Y+Z}$, but different luminance Y: $P_R \sim Y$, $P_G \sim Y$ and $P_B \sim Y$. When using color targets with an almost constant reflectivity in function of wavelength (e.g. 'neutral' colors of the MBCCC), and with the added desire to optimize the dynamic range of each color channel separately for the given light source, this becomes $P_R = P_G = P_B = Y/100$ (gray balancing). This process is actually a kind of normalization of RGB values with regard to the light source.
Practically the camera color dependent gain factors g_R^{cam} and g_B^{cam} are adjusted first so that gray balance is obtained for the MBCCC 'white' target using a simple bisection root finding method. Hereafter the lookup-table (LUT) is constructed in order to achieve gray balance for the 5 other MBCCC 'neutral' color targets with luminance ranging from 3.1 to 59.1.

3.6. The RGB to sRGB transforms

If the camera sensor spectral sensitivities are equal to or a linear combination of the CIE $\bar{x}\,\bar{y}\,\bar{z}$ color matching functions, i.e. it is a colorimetric device, then the relationship between the input RGB and the $sRGB$ color space would simply be linear because the sRGB space is linearly related to the CIE XYZ space. This is generally not the case, and leads to a type of metamerism in which two colors which look the same as seen by the camera (same RGB values) but may look different as seen by a human observer (different $sRGB$ and XYZ values) under the same lighting conditions. It is clear that although we can try to model the non-linear relationship between the RGB and $sRGB$ color space with higher-order transforms we will not be able to compensate for this type of machine-human metamerism. The RGB to $sRGB$ transform Γ of order m can be written as:

$$\begin{pmatrix} S_R \\ S_G \\ S_B \end{pmatrix} = \Gamma_m \begin{pmatrix} P_R \\ P_G \\ P_B \end{pmatrix} = \begin{pmatrix} \Theta_m\,(\,P_R \quad P_G \quad P_B\,) \\ \Theta_m\,(\,P_R \quad P_G \quad P_B\,) \\ \Theta_m\,(\,P_R \quad P_G \quad P_B\,) \end{pmatrix} \begin{pmatrix} a_{1,R} & \cdots & a_{1,B} \\ \vdots & & \vdots \\ a_{m,R} & \cdots & a_{m,B} \end{pmatrix}, \tag{4}$$

whereby $(\,S_R \quad S_G \quad S_B\,)$ are the linear $sRGB$ values and the operator Θ_m transforms a 3 element row vector to an m element row vector according to the order of the transform m. Several transforms were tested:

$$\begin{aligned}
\Theta_3\,(\,P_R \quad P_G \quad P_B\,) = \quad & (\,P_R \quad P_G \quad P_B\,) \\
\Theta_6\,(\,P_R \quad P_G \quad P_B\,) = \quad & (\,P_R \quad P_G \quad P_B \quad P_RP_G \quad P_GP_B \quad P_BP_R\,) \\
\Theta_8\,(\,P_R \quad P_G \quad P_B\,) = \quad & (\,1 \quad P_R \quad P_G \quad P_B \quad P_RP_G \quad P_GP_B \quad P_BP_R \quad P_RP_GP_B\,) \\
\Theta_9\,(\,P_R \quad P_G \quad P_B\,) = \quad & (\,P_R \quad P_G \quad P_B \quad P_RP_G \quad P_GP_B \quad P_BP_R \quad P_R^2 \quad P_G^2 \quad P_B^2\,) \\
\Theta_{11}\,(\,P_R \quad P_G \quad P_B\,) = \quad & (\,1 \quad P_R \quad P_G \quad P_B \quad P_RP_G \quad P_GP_B \quad P_BP_R \quad P_R^2 \quad P_G^2 \quad P_B^2 \quad P_RP_GP_B\,)
\end{aligned} \tag{5}$$

Determination of the coefficients a_{ij} of the transform Γ_m is based on the 24 MBCCC targets. Their $L^*a^*b^*$ 2 degree observer values $(\,T_{L,i} \quad T_{a,i} \quad T_{b,i}\,)$ were measured under D65 lighting using a Gretag[§] SPM50 spectrophotometer.

[§]GretagMacbeth AG, Althardstrasse 70, CH-8105 Regensdorf, Switserland

We now define the non-linear operator Λ which transforms tristimuli from the $sRGB$ space to the $L^*a^*b^*$ space via the XYZ space (see fig. 2).

$$\begin{pmatrix} T_L \\ T_a \\ T_b \end{pmatrix} = \Lambda \begin{pmatrix} S_R \\ S_G \\ S_B \end{pmatrix} = \begin{pmatrix} 0 & \lambda_Y & 0 \\ \alpha_X & \alpha_Y & 0 \\ 0 & \beta_Y & \beta_z \end{pmatrix} \begin{pmatrix} 41.2 & 35.8 & 18.0 \\ 21.3 & 71.5 & 7.2 \\ 1.9 & 11.9 & 95.0 \end{pmatrix} \begin{pmatrix} S_R \\ S_G \\ S_B \end{pmatrix} . \tag{6}$$

The first matrix on the right-side contains the XYZ to $L^*a^*b^*$ transform under D65 lighting as defined by the CIE:

$$\begin{array}{rl} \lambda_Y(t) = & 116f(t/100.0) - 16 \\ \alpha_X(t) = & 500f(t/95.0) \\ \alpha_Y(t) = & -500f(t/100.0) \\ \beta_Y(t) = & 200f(t/100.0) \\ \beta_Z(t) = & -200f(t/108.0) \\ f(t) = & \begin{cases} 7.787t + \frac{16}{116} & \text{if } t < 0.008856 \\ t^{1/3} & \text{if } 0.008856 \leq t \leq 1 \end{cases} . \end{array} \tag{7}$$

This operator can be inverted, and is used to determine the target values for the RGB to $sRGB$ transform Γ:

$$\begin{pmatrix} S^M_{R,i} \\ S^M_{G,i} \\ S^M_{B,i} \end{pmatrix} = \Lambda^{-1} \begin{pmatrix} T^M_{L,i} \\ T^M_{a,i} \\ T^M_{b,i} \end{pmatrix}, i = 1, \cdots, 24 . \tag{8}$$

Replacing $(S_R \quad S_G \quad S_B)$ by the measured values $(S^M_{R,i} \quad S^M_{G,i} \quad S^M_{B,i})$ of the MBCCC targets in equation 4 leads to 3 sets of overdetermined linear equations which can easily be solved in a least-squares sense using e.g. singular-value decomposition (SVD):

$$\begin{pmatrix} S^M_{c,1} \\ \vdots \\ S^M_{c,24} \end{pmatrix} = \begin{pmatrix} \Theta_m (P_{R,1} & P_{G,1} & P_{B,1}) \\ & \vdots & \\ \Theta_m (P_{R,24} & P_{G,24} & P_{B,24}) \end{pmatrix} \begin{pmatrix} a_{1,c} \\ \vdots \\ a_{m,c} \end{pmatrix} \quad c = R, G, B . \tag{9}$$

Unfortunately, this solution is only mathematically optimal as the linear $sRGB$ color space is hardly suited to measure color differences as seen by a human observer. This can be achieved by minimizing the sum of squared errors of the transform in $L^*a^*b^*$ space:

$$\exists \Gamma^{Lab}_m, \forall \Gamma_m : \sum_{i=1}^{24} \| \begin{pmatrix} T^M_{L,i} \\ T^M_{a,i} \\ T^M_{b,i} \end{pmatrix} - \Lambda\Gamma^{Lab}_m \begin{pmatrix} P_{R,i} \\ P_{G,i} \\ P_{B,i} \end{pmatrix} \|^2 \leq \sum_{i=1}^{24} \| \begin{pmatrix} T^M_{L,i} \\ T^M_{a,i} \\ T^M_{b,i} \end{pmatrix} - \Lambda\Gamma_m \begin{pmatrix} P_{R,i} \\ P_{G,i} \\ P_{B,i} \end{pmatrix} \|^2 . \tag{10}$$

The above equation is solved with the Nelder-Mead simplex algorithm,[17] using the SVD solution as an initial guess. It is of course logical that the performance in terms of average ΔE of the transforms on the training set gets better with m, especially those using non-linear optimization (see fig. 3). The improvement is, however, not very spectacular compaired to the increasing number of terms in the transforms. The non-linearly optimized transforms Γ^{Lab}_m always have a lower average ΔE than their linearly solved counterparts Γ_m, but their maximal errors are higher except for $m = 11$ and $m = 14$. The use of the ∞-metric (max-metric) instead of Euclidean metric in $L^*a^*b^*$ space was also tried, but resulted in significantly higher average errors for a marginal gain in the maximal error. The simplex algorithm also needed much more iterations for convergence with the ∞-metric.

4. CHECKING AND ADJUSTING AN EXISTING ACQUISITION SYSTEM PROFILE

Once a profile is determined and stored it can be used as long as the acquisition system doesn't change too much (aging of the light source bulb, changes in CCD sensor spectral response, ...). This is easily checked by comparing the $L^*a^*b^*$ value of a test target (MBCCC 'white') with its value during the calibration procedure. We set a limit of 1 ΔE^*_{ab} unit as the maximum deviation for the acceptance of the profile.
Of more concern is the changing response of the acquisition system in function of the warmup-time (see fig. 4): even though the system more or less stabilizes after about 20 minutes, the blue response continues to change and diverges

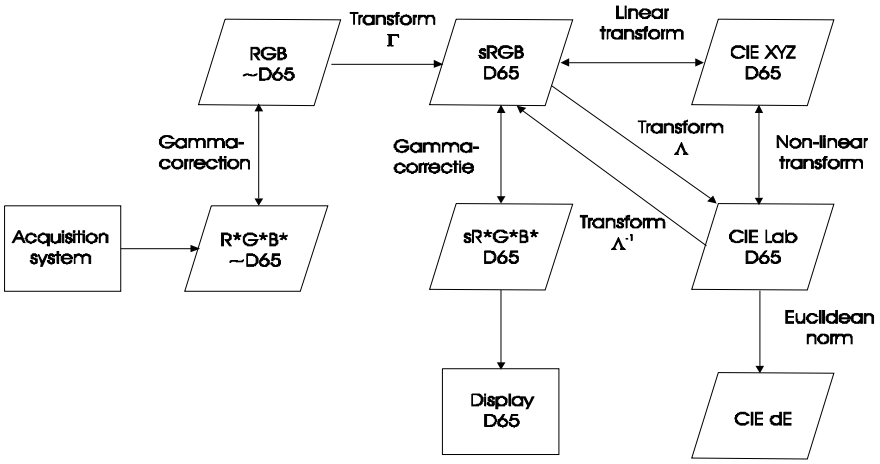

Figure 2. The different color spaces of the calibration scheme and their relations.

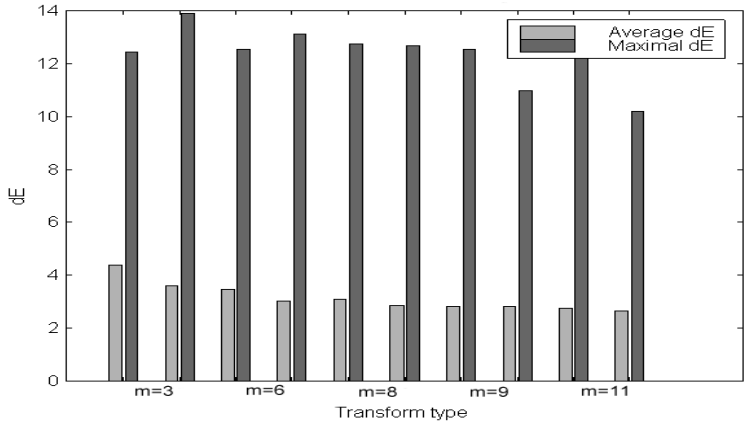

Figure 3. The performance of the transforms on the training set. Transforms are grouped by order m, with the linearly solved one on the left, and the non-linearly optimized one on the right.

from the red and green response. The profile used here was determined after a warmup-time of around 60 minutes. It is clear an increasing difference between the calibration and the measurement time results in an increasing error, even though these remain generally small enough for the acceptance of the profile. Assuming that the non-linearity of the acquisition system doesn't change with slight changes in the frame grabber gain g^{fg} and camera color dependent gains g_R^{cam} and g_B^{cam}, i.e. assuming the linearizing LUT and the transform Γ remain valid, we can adjust these parameters on the fly when checking a profile. This doesn't involve any extra interaction as the same test target is used, and markedly improves the precision.

The image used for checking the profile is also used for multiplicative shading correction. This corrects for spatial inhomogeneities in the lighting. Images acquired with a validated and adjusted profile are transformed to the gamma-corrected $sR^*G^*B^*$ space before they are stored, see fig. 2. This is called output rendering and should provide a fairly realistic image on any modern CRT-based monitor which has its white-point set at 6500 K.[18]

5. EXPERIMENTAL RESULTS AND DISCUSSION

5.1. Accuracy

With accuracy we mean the consistency with which measurements of colors are close their real measured values, as measured by a reference instrument, e.g. a spectrophotometer. Good accuracy will be especially important when exchanging images. A test target set was constructed consisting of 15 plastic and paper samples, as well as 12 skin areas (normal Caucasian and Asian skin, moles, pimples, ...) from human volunteers. The samples were measured

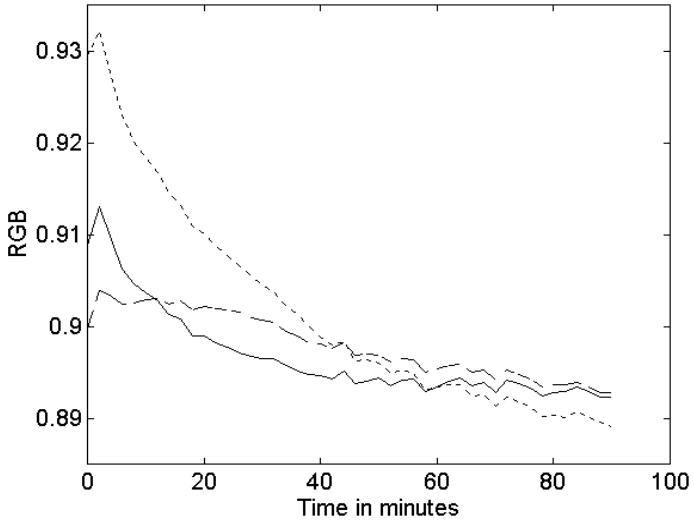

Figure 4. The R (solid line), P (dashed line) and B (dotted line) response of the white MBCCC target in function of the warmup-time of the acquisition system.

with a Gretag SPM50 spectrophotometer as well as imaged with the proposed acquisition system. Pixels in these images were averaged over an area roughly corresponding to the measurement area of the spectrophotometer (circle of 5mm diameter), and compared in the $L^*a^*b^*$ space for each of the possible transforms Γ_m. In contrast to the

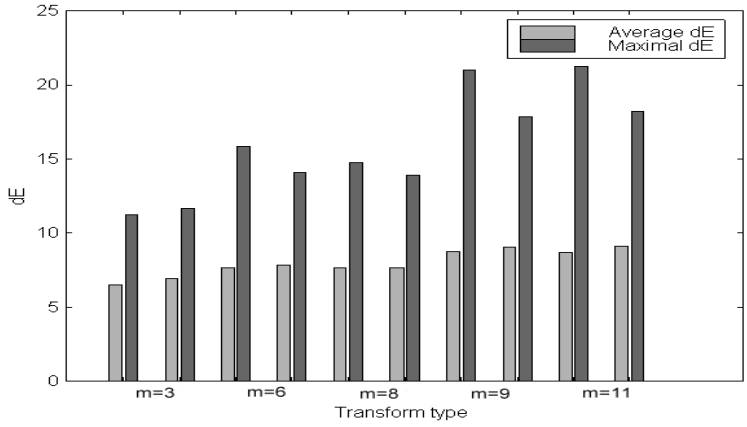

Figure 5. The performance of the transforms on the test set. Transforms are grouped by order m, with the linearly solved one on the left, and the non-linearly optimized one on the right.

performance of the transforms Γ_m on the training set, see fig. 3, the simplest transform Γ_3 performs best on the test set, see fig. 5. The reason is that the training set is actually much to small for the higher order transforms, and this can lead to uncontrolled, oscillating behavior in the space between the points of the training set. In that respect Γ_3 and Γ_3^{Lab} are much better behaved, and the preferred solutions if one wants to keep a simple and quick calibration procedure for the acquisition system, i.e. one which uses relatively few training targets. Although the non-linearly optimized transforms have slightly worse performance than their linearly solved counterparts in terms of average and maximal ΔE^*_{ab}, the errors on the individual targets do not fluctuate as much. This effect is more pronounced for higher-order transforms and almost non-existent for $m = 3$. In conclusion we may say that Γ_3 is most suited for our case, with $\langle \Delta E^*_{ab} \rangle = 6.53$ and $\Delta E^*_{ab} < 11.2$.
It is also important to note that the 'skin' targets (numbered from 16 to 28) show the same range of ΔE errors as

the paper and plastic targets (numbered from 1 to 15), see fig. 6, even if their spectra maybe completely different from the ones used to determine the transforms (MBCCC targets consist of dyed cardboard squares). This shows that the machine-human metamerism problem is probably not an issue for skin imaging.

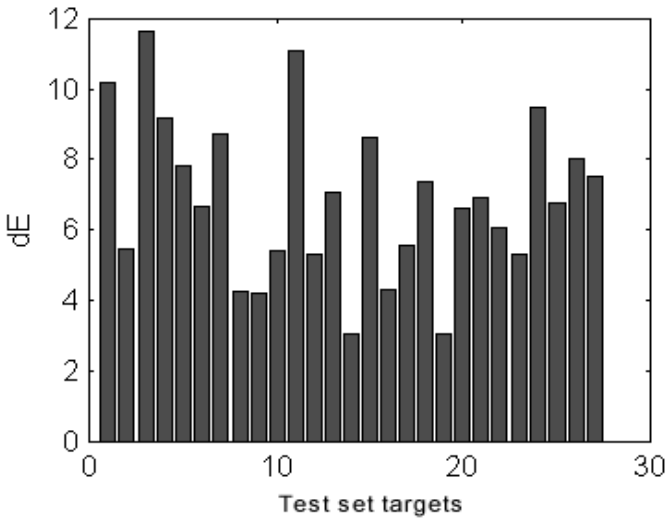

Figure 6. The performance of the linearly solved 3-term transform Γ_3.

5.2. Precision

With precision we describe the reproducibility of measurements, or the way repeated measurements are spreaded around the average of those measurements. Precision will be important for any quantitative measurement of image color characteristics. We can distinguish several types of precision: short-term precision when making several consecutive measurements of the same target, medium-term or profile precision when comparing measurements made under one profile, and long-term or inter-profile precision when talking about the agreement between measurements made under different profiles.

Short term precision based on 20 consecutive measurements of the MBCCC 'white' target was very good: $\langle \Delta E^*_{ab} \rangle = 0.04$, with $\Delta E^*_{ab} < 0.1$. The results for the medium-term and long-term precision can be seen in fig. 7. Here the average error $\langle \Delta E^*_{ab}(t) \rangle$ for each target was computed with regard to the average sample $L^*a^*b^*$ value of the target (10 and 9 measurements respectively). To simulate possible long-term changes in the acquisition system, the color temperature of the light source was modified for half of the profiles. There was no noticeable difference in precision between profiles for the normal and modified acquisition system. The average, standard deviation and maximal errors over all the MBCCC targets for medium-term and long-term precision are $\langle \Delta E^*_{ab} \rangle = 0.34$, $s = 0.094$ with $\Delta E^*_{ab} < 1.2$, and $\langle \Delta E^*_{ab} \rangle = 0.30$, $s = 0.10$ with $\Delta E^*_{ab} < 1.2$ respectively. The fact that the long-term precision is slightly better than the medium-term precision might be explained by the fact that any measurements for the long-term precision were made directly after the profile was determined, thereby avoiding the drift problems outlined in fig. 4.

5.3. In vivo measurements

Images of the skin before its removal were acquired during a histological study of melanin migration under influence of UV-radiation. Using a MANOVA procedure and Wilk's Lambda we tried to asses the significance of color differences of visually homogenous regions of interest (ROI's). This method assumes normally distributed populations, so it is only valid if enough pixels are present in a ROI because we have no idea of the real distribution of the individual pixels. Strictly speaking it can only be used to compare ROI's in the same image or in images acquired quickly after each other because of the precision of the acquisition system which may induce a bias on the average, but has almost no effect on the variance of the pixel population.

We found that starting from populations of 600 to 700 pixels (equivalent to about $0.5mm^2$ of skin area) any difference

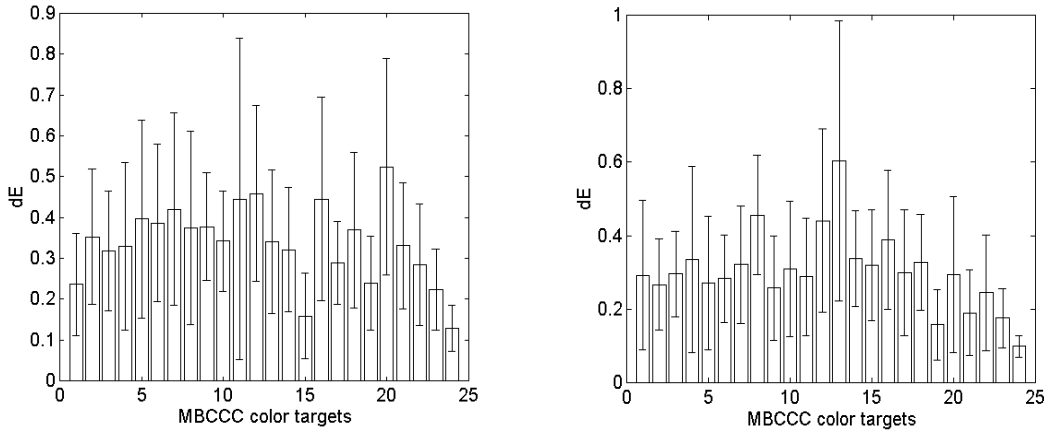

Figure 7. The average ΔE of the MBCCC color targets under the same (left) and different (right) profiles. The error bars represent one standard deviation

of more than 1 ΔE^*_{ab} unit is significant at the $p = 0.01$ level. As this is the theoretical just noticeable difference (JND) between two colors, this probably has more to do with our (in)ability to delineate visually homogenous ROI's than the noise characteristics of the acquisition system.
In conclusion we may say that when comparing large enough visually homogenous ROI's between images any difference in the average pixel value of more than $2 - 3\ \Delta E^*_{ab}$ is significant. This limit may of course be higher when comparing visually inhomogeneous ROI's. To put this in perspective, the erythema that appeared on some volunteers 2 days after UV-exposure showed a difference of more that $20\Delta E^*_{ab}$ units with unexposed skin.

6. CONCLUSIONS

We have proposed a small field-of-view color image acquisition system which allows colorimetrically consistent acquisition of digital images. These images are stored in a standard color space with known primaries and white-point, and as such can be exchanged and compared with other images defined in the same color space, even if acquired by other means. They are readily displayable on CRT-based displays.
The system has good precision and medium accuracy, and its use for in vivo evaluation of the skin should pose no problem.

7. ACKNOWLEDGMENT

This project is funded by the FWO in Belgium, ref. F7801

REFERENCES

1. G. E. Healey and R. Kondepudy, "Radiometric CCD camera calibration and noise estimation," *IEEE Transcations on Pattern Analysis and Machine Intelligence* **16**(3), pp. 267–276, 1994.
2. Y.-C. Chang and J. F. Reid, "RGB calibration for color image analysis in machine vision," *IEEE Transactions on Image Processing* **5**(10), pp. 1414–1422, 1996.
3. B. A. Wandell, "The synthesis and analysis of color images," *IEEE Transactions on Pattern Analysis and Machine Intelligence* **PAMI-9**(1), pp. 2–13, 1987.
4. D. Slater and G. Healey, "The illumination-invariant recognition of 3d objects using local color invariants," *IEEE Transactions on Pattern Analysis and Machine Intelligence* **18**(2), pp. 206–210, 1996.
5. G. Finlayson, "Color in perspective," *IEEE Transactions on Pattern Analysis and Machine Intelligence* **18**(10), pp. 1034–1038, 1996.

6. G. D. Finlayson and M. S. Drew, "White-point preserving color correction," in *Fifth Color Imaging Conference: Color Science, Systems and Applications*, pp. 258–261, IS&T, SID,, 1997.
7. E. Boldrin, P. Campadelli, and R. Schettini, "Learning colkor appearance models," in *Fifth Color Imaging Conference: Color Science, Systems and Applications*, pp. 173–176, IS&T, SID,, 1997.
8. P. M. Hubel, J. Holm, G. D. Finlayson, and M. S. Drew, "Matrix calculations for digital photography," in *Fifth Color Imaging Conference: Color Science, Systems and Applications*, pp. 105–111, IS&T, SID,, 1997.
9. H. Kang, *Color Technology for Electronic Imaging Devices*, SPIE Optical Engineering Press, 1997.
10. N. Cascinelli et al., "A possible tool for clinical diagnosis of melanoma: The computer," *Journal of the American Academy of Dermatology* **16**(2, Part 1), pp. 361–367, 1987.
11. J. L. Stone, R. L. Peterson, and J. E. Wolf, "Digital imaging techniques in dermatology," *Journal of the American Academy of Dermatology* (5, part 1), pp. 913–917, 1990.
12. R. Kenet et al., "Clinical diagnosis of pigmented lesions using digital epiluminescence microscopy," *Arch. of Dermatology* **129**, pp. 157–174, 1993.
13. W. Stolz et al., "Improvement of monitoring of melanocytic skin lesions with the use of a computerized acquisition and surveilland with a skin surface microscopic television camera," *Journal of the American Academy of Dermatology* **35**(2, Part 1), pp. 202–207, 1996.
14. T. Schindewolf et al., "Evaluation of different image acquisition techniques for a computer vision system in the diagnosis of malignant melanoma," *Journal of the American Academy of Dermatology* **31**(1), pp. 33–41, 1994.
15. M. Nischik et al., "Analysis of skin erythema using true-color images," *IEEE Trans. On Medical Images* **16**(6), pp. 711–715, 1997.
16. G. Holst, *CCD arrays, Cameras and Displays*, SPIE Optical Engineering Press, 1996.
17. W. H. Press, *Numerical Recipes in C: The Art of Scientific Computing*, Cambridge Univ. Press, 1993.
18. J. Holm, "Issues relating to the transformation of sensor data into standard color spaces," in *Fifth Color Imaging Conference: Color Science, Systems and Applications*, pp. 290–295, IS&T, SID,, 1997.